ADVANCED FUNCTIONAL MATERIALS

FULL PAPER

DOI: 10.1002/adfm.200500629

Capillary Force Lithography: Fabrication of Functional Polymer Templates as Versatile Tools for Nanolithography**

By *Christiaan M. Bruinink*, *Mária Péter*, *Pascale A. Maury*, *Meint de Boer*, *Laurens Kuipers*, *Jurriaan Huskens*,* and *David N. Reinhoudt**

The implementation of high-resolution polymer templates fabricated by capillary force lithography (CFL) is explored both in nanoimprint lithography (NIL) and in the wet-etching of metals. Several different thermoplastic and UV-curable polymers and types of substrates are incorporated into the general CFL procedure to meet the diverging requirements of these two applications. The mechanical stability of UV-curable templates for imprinting in polymers, as examined by atomic force microscopy (AFM), and their anti-adhesive properties are excellent for application in NIL. The conditions for curing the UV-curable polymer are optimized in order to obtain high-stability polymer templates. Gold patterns on silicon with a lateral resolution of 150 nm are fabricated by subsequent lift-off in acetone. Similar patterns with a lateral resolution of 100 nm are fabricated using templates of thermoplastic polymers on gold layers on silicon as an etch mask. The transfer of stamp residues during CFL with these polymer templates is proven by X-ray photoelectron spectroscopy (XPS) and AFM friction analysis. For poly(methylmethacrylate) (PMMA), the presence of large amounts of silicon-containing residues is found to compromise the processability of the resulting template in subsequent O_2 reactive-ion etching (RIE) treatment. The extent of silicon contamination is up to six times less for polystyrene (PS). At this level, the etch performance of the PS etch mask is not affected, as was the case for PMMA. Accurate downscaling of the lateral dimensions of the resulting metal patterns by several factors with respect to the dimensions of the PS etch mask is achieved by over-etching of the gold. Overall, the results in this paper demonstrate the potential of CFL templates as tools for high-resolution soft lithography.

1. Introduction

The development of low-cost, high-throughput lithographic techniques for the fabrication of sub-100 nm patterns has taken a dominant position in nanofabrication during the last decade. The unrelenting efforts that are undertaken in this field are the result of the corresponding high cost and low accessibility of state-of-the-art lithographic techniques—for example, deep-UV and extreme-UV photolithography,[1] soft X-ray lithography,[2] electron-beam writing,[3] and ion-beam lithography[4]—that are still entailed for large-area fabrication of high-resolution patterns. Although these techniques will remain the main technology for the semiconductor industry, soft lithography[5] and nanoimprint lithography (NIL)[6] have made enormous progress as non-photolithographic techniques in several areas of exploratory and scientific research in terms of sub-100 nm resolution, reproducibility, and uniformity of the patterns over large areas. Generally, the concept of these non-photolithographic techniques lies in the exact replication of the structures on a master by (conformal) contact with the substrate of interest. To overcome the reliance on expensive state-of-the-art equipment for the fabrication of the necessary high-resolution masters, several innovative strategies have been put forward that extend the capabilities of soft lithography and NIL into the sub-100 nm range. These inexpensive strategies basically exploit the combination of different (aspects of) soft-

[*] Prof. J. Huskens, Prof. D. N. Reinhoudt, C. M. Bruinink, Dr. M. Péter, P. A. Maury
Laboratory of Supramolecular Chemistry and Technology
MESA+ Institute for Nanotechnology, University of Twente
P.O. Box 217, 7500 AE Enschede (The Netherlands)
E-mail: j.huskens@utwente.nl; d.n.reinhoudt@utwente.nl
Prof. J. Huskens
Strategic Research Orientation 'Nanofabrication'
MESA+ Institute for Nanotechnology, University of Twente
7500 AE Enschede (The Netherlands)
M. de Boer
Transducers Science and Technology Group
MESA+ Institute for Nanotechnology, University of Twente
7500 AE Enschede (The Netherlands)
Prof. L. Kuipers
Strategic Research Orientation 'Advanced Photonic Structures'
MESA+ Institute for Nanotechnology, University of Twente
7500 AE Enschede (The Netherlands)
Prof. L. Kuipers
FOM Institute for Atomic and Molecular Physics (AMOLF)
Kruislaan 407, 1098 SJ Amsterdam (The Netherlands)

[**] This research was supported by the MESA+ Institute for Nanotechnology and is part of the Strategic Research Orientation 'Advanced Photonic Structures'. Of CMAL/MESA+, Mark A. Smithers is acknowledged for operating the high-resolution SEM, Emiel Speets and Albert van den Berg for conducting the XPS analyses. Special thanks go to MicroResist Technology GmbH (Germany), and specifically to Gerhard Bleidiessel, for donation of the UV-curable polymer mr-L 6000 and technical support. Finally, Dominique Altpeter and Gerrit Boom of the MESA+ cleanroom are acknowledged for constructive scientific discussions.

and/or photolithographic techniques in order to downscale the feature sizes of the master. From the ever-increasing list of existing strategies, the most promising set of lithographic techniques to date is edge lithography. The general feature that relates the lithographic techniques in this set is the translation of the structural characteristics of the master into resultant edge patterns. Edge-lithographic techniques include near-field phase-shift photolithography,[7] maskless lithography,[8] undercutting by isotropic wet-etching,[9] patterning local disorder in monolayer resists,[10] and edge-spreading lithography.[11] The development of these techniques has led to the facile fabrication of features with ultimate lateral sizes of down to 50 nm.

Recently, we have reported a novel variant of edge lithography by combining capillary force lithography (CFL)[12] with replica molding (REM)[5] for the fabrication of second-generation stamps suitable for conducting high-resolution soft lithography.[13] CFL is an emerging, non-photolithographic technique that combines the essential feature of NIL—molding a polymer melt—with the key element of soft lithography—molding with an elastomeric stamp for large-area patterning of polymer films.[14] At a temperature (T) above the glass-transition temperature (T_g) of the polymer, capillary forces drive the polymer to conform to the mold pattern. The initial polymer film thickness and the feature dimensions of the mold determine the type of the resulting polymer patterns. CFL of thick polymer layers results in a negative copy of the mold, with a residual layer that remains on the substrate. Upon decreasing the initial polymer film thickness, the meniscus cannot rise to completely fill the spaces between the mold and the substrate, owing to polymer insufficiency. Although no special attention was given to the latter structures by Lee and co-workers,[12] we have been investigating the potential of these high-resolution polymer templates in edge lithography, for example, the use of these templates as masters in soft lithography (Fig. 1, route A). Application of the resulting stamps in microcontact printing (μCP) resulted in patterned self-assembled monolayers (SAMs) and gold structures after subsequent wet-chemical etching, with a resolution of ca. 125 nm.[13]

Here, we report recent developments in using CFL as a nanofabrication technique by utilizing the CFL polymer templates in two additional patterning techniques (Fig. 1). We discuss the applicability of the polymer templates as molds for NIL (Fig. 1, route B) and as etch masks for the selective wet-etching of metals (Fig. 1, route C) by incorporating UV-curable polymers and the use of gold on silicon substrates in the CFL procedure, respectively. The (mechanical) stability and integrity of the template during processing and the ultimate resolution of the resulting metal patterns are of prime importance in our process evaluation, which was carried out with atomic force microscopy (AFM) and scanning electron microscopy (SEM). Therefore, emphasis was placed on the process conditions and the etch behavior of the polymer templates (and of the underlying substrate) in order to achieve these goals.

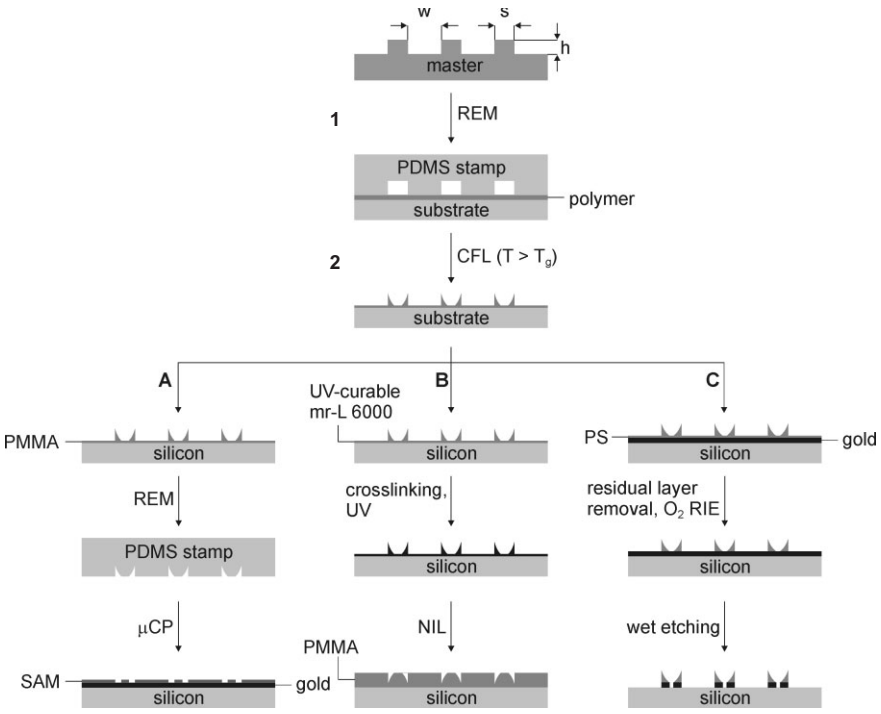

Figure 1. Schematic representation of the general, two-stage CFL procedure for the fabrication of high-resolution polymer templates. 1) REM of the first-generation silicon master to poly(dimethylsiloxane) (PDMS) stamps (width, w: 5 μm, spacing, s: 3 μm, and height, h: 1.2 μm); 2) CFL [12] on thin polymer layers at $T > T_g$ of the polymer for several hours. After cooling at room temperature and releasing the stamp, the resulting submicrometer polymer templates can fulfill different functions, depending on the type of polymer and substrate: A) template as master for stamp fabrication; B) template as mold for NIL; C) template as etch mask for the wet-etching of metals. PMMA: poly(methyl methacrylate); SAM: self-assembled monolayer; RIE: reactive-ion etching; μCP: microcontact printing; PS: polystyrene.

2. Results and Discussion

2.1. Fabrication of High-Resolution, Functional Polymer Templates

The top part of Figure 1 depicts the basis of our soft-lithographic procedure for generating high-resolution polymer features on substrates by CFL. A liquid prepolymer of poly(dimethylsiloxane) (PDMS) was cast against a silicon master. All the masters in our study were fabricated by standard photolithography and contain either continuous (lines) or discontinuous (pillars) features of micrometer size (width, $w = 5$ μm, spacing, $s = 3$ μm, height, $h = 1.2$ μm). The PDMS stamps were cured for 1–18 h at 60 °C in order to obtain stamps of minimal (ca. 0.5 N mm^2) to medium (ca. 2 N mm^2) modulus,[15] respectively, suitable for conducting CFL. Placing these PDMS

ADVANCED FUNCTIONAL MATERIALS

stamps onto any substrate at room temperature led to intimate physical contact over large areas. Special care was taken to prevent the interference of dust particles by contacting the substrate and stamp with minimal delay. Larger dust particles in particular were found to act as sites at which conformal contact was gradually lost during CFL.

High-temperature processing is known to limit the performance of PDMS stamps.[12] Without taking proper precautions, the contact between the substrates and PDMS stamps cannot withstand the thermal stresses that build up owing to differences in thermal expansion coefficients ($a_{PDMS} \gg a_{Si}$). To prevent separation, the thickness of the PDMS stamps was kept down to about 1 mm, in order to ensure sufficient flexibility. This measure was found to improve the overall performance of commercial PDMS for CFL processing of polymer layers effectively, even though the stamp hardens further by thermal curing during processing.

To obtain high-resolution polymer templates, thin polymer layers (ca. 35–200 nm) were spun onto silicon substrates. At this range of polymer film thicknesses, no dewetting effects by physical confinement—which could impair the alignment of the polymer features at the feature edges of the PDMS stamp—were to be expected.[16] The initial conditions for CFL on thin polymer layers are crucial for the formation of useful symmetrical template structures. Of all the different procedures, pre-equilibration of the PDMS stamp and the substrate to the annealing temperature before bringing the PDMS stamp into conformal contact with the substrate was found to result in the most-symmetrical polymer structures over large areas.[13] The annealing temperature T was set sufficiently above T_g ($T \approx T_g + 40\,^{\circ}C$) in order to ensure polymer mobility for patterning the polymer layers during CFL. Typical annealing times were chosen in the range 2–20 h.

Capillary kinetics of a polymer melt in permeable microchannels[17] have been shown to depend on several parameters, such as time, polymer flow (temperature, type of the polymer, wetting capabilities of the stamp), and the amount of polymer accessible to fill the spaces between the mold and the substrate (initial polymer film thickness, fill factor of the stamp). As a result, one can expect to have control over the lateral and vertical dimensions of the resultant polymer features by changing any of these parameters. Figure 2 shows the result of increasing the initial polymer film thickness from 35 nm to 150 nm while the other process parameters were kept constant (polystyrene (PS), weight-average molecular weight $M_w = 240$ kDa ($1\ \text{Da} = 1.66 \times 10^{-27}$ kg), 150 °C, 20 h, PDMS stamp with 5 μm × 3 μm line-and-space pattern).

Cross-sectional AFM analyses of the resultant PS templates (Fig. 2d) revealed that it is possible to exert certain control over the feature line width of the polymer template, ranging in this case from 440 to 850 nm (Fig. 2a–c). Adjusting the other process parameters should result in polymer templates with an even larger range of feature widths. Under the present process conditions, a thin residual layer of < 100 nm is always present in the template, protecting the underlying substrate from direct post-processing (Fig. 2e).

In contrast to our previous procedure,[13] it was found by optical inspection that cooling the stamp and substrate for 5 s (instead of 30 min) at room temperature was already sufficient to release the stamp from the substrate without generating (microscopic) distortions to the polymer template. After every process step, the templates and substrates were examined by AFM and/or SEM to obtain information about the mechanical stability of the template during processing and the pattern-transfer fidelity of the patterning technique to the substrate, respectively.

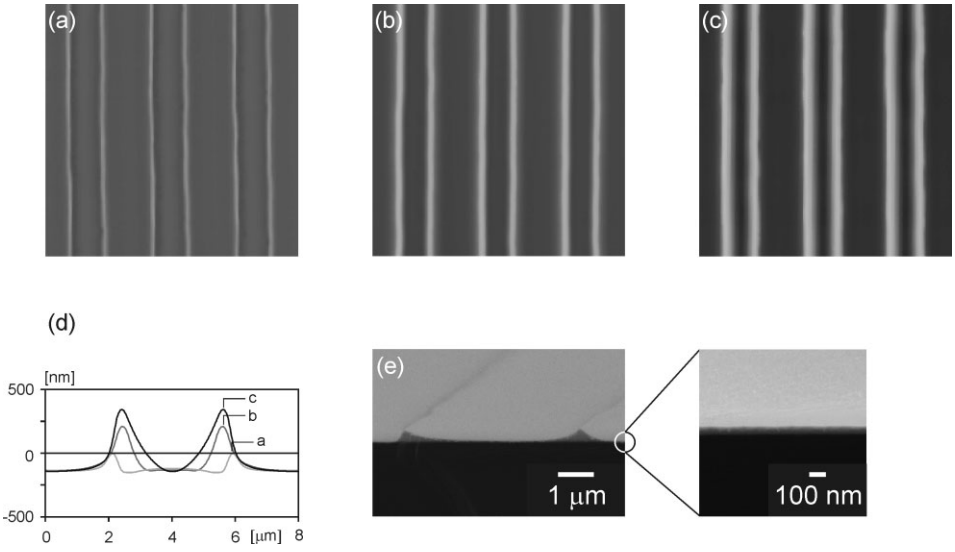

Figure 2. Contact-mode (CM)-AFM height images (*z* range: 1000 nm; image size: 25 μm × 25 μm) of different high-resolution polymer (PS) templates. The polymer templates were fabricated by CFL on initial polymer thicknesses of a) 35, b) 80, and c) 150 nm at 150 °C for 20 h. d) The feature widths (full width at half maximum, FWHM) of these PS structures, respectively 440, 680, and 850 nm, were determined from the average height cross-sectional analysis of the respective meniscus of each template. e) SEM image of a cross-sectional view of a symmetrical polymer template on silicon. From the close-up SEM image, a thin residual layer is seen on the silicon substrate.

2.2. CFL Templates as High-Resolution Molds for NIL

The requirements for polymer templates that can successfully function as robust NIL molds (Fig. 1, route B) are more stringent than for use as masters for μCP stamp fabrication (Fig. 1, route A), because the imprint conditions in standard NIL processing schemes demand the template to be resistant to high temperatures—in the range of 70 to 80 °C above the T_g of the polymer—and high pressures for several minutes. To date, only low-viscosity thermoplastic polymers, for example, poly(methylmethacrylate) (PMMA), PS, and some block copolymers have been exploited in CFL. However, the CFL process is universal in that it also allows the patterning of other types of polymers, for example, UV-curable polymers. The use of this type of polymer offers the advantage over thermoplastic polymers of post-processing stabilization of the polymer template by UV crosslinking (Fig. 3a).

The commercially available UV-curable polymer mr-L6000 (Microresist Technology GmbH, Germany) is a chemically amplified negative-tone photoresist with a very low T_g (35 °C), permitting moderate processing conditions for patterning by CFL (T = 70 °C, 2 h). Special care was taken so that, prior to UV exposure, the mr-L6000 substrate was not exposed to white light (i.e., processing was carried out in a yellow-light environment). Cross-sectional AFM analysis of a representative mr-L6000 template (Fig. 3b) reveals the typical transient meniscus (W-shaped) of capillary rise.[18,19] It has been shown that i) any meniscus evolves in a uniform U-shape upon long annealing times,[18] and ii) splitting of the meniscus may give rise to exposure of the underlying substrate in the noncontact areas.[19] Therefore, the observation of a transient meniscus in our template implies that, under the present processing conditions, the polymer pattern could not fully develop the characteristic U-shape meniscus.

UV crosslinking of mr-L6000 templates typically involves a flood-exposure in a UV-exposure system, followed by a post-exposure bake on the hotplate. For an exposure dose of 360 mJ cm^{-2} and a post-exposure bake at 100 °C for 10 min, the structural integrity of the template was not affected by the post-processing stabilization procedure (Fig. 3b and c, template height is ca. 100 nm and the full width at half maximum, FWHM, is ca. 400 nm). UV exposure of this type of resist activates a photoacid generator responsible for releasing an acid that initiates the cationic polymerization of the epoxy resist upon heating. At this stage, both crosslinking and thermal flow may occur simultaneously, which can have a significant effect on the pattern fidelity upon curing, in particular when thermal flow dominates over crosslinking.[20] The results shown in Figure 4 are the outcome of an AFM study that was carried out in order to address the interplay between these two processes during a post-exposure bake at 100 °C for 10 min following exposure at different doses.

The response of unexposed mr-L6000 templates to thermal treatment excludes the interference of thermal crosslinking with the stabilization of polymer patterns during UV crosslinking at 100 °C (Fig. 4a). Figure 4 illustrates a clear trend in pattern stability, in terms of feature height and width, as a function of the exposure dose. At low exposure doses, thermal flow was the dominating process, causing significant sagging of the features on the template (Fig. 4b). Upon increasing the exposure dose (Fig. 4c) the template structures became more and more heat resistant, up to the point where the feature dimensions were independent of the exposure dose (Fig. 4d). At these high exposure doses the polymer template was resistant to thermal flow, as crosslinking was the dominating process in this regime. The critical exposure dose of ca. 100 mJ cm^{-2}, at which UV crosslinking of the polymer template is still successful, was esti-

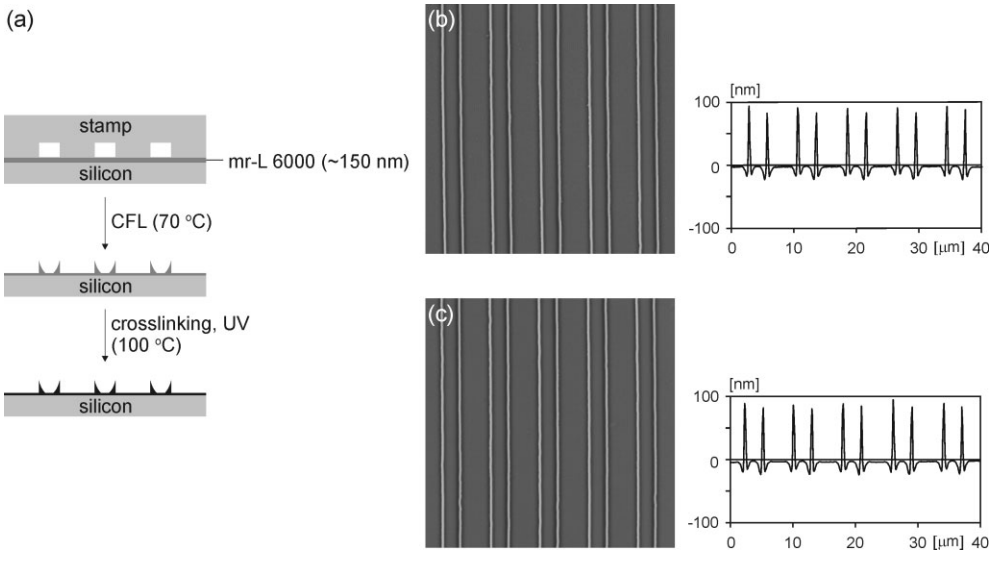

Figure 3. a) Schematic representation of the CFL procedure for the fabrication of NIL molds using the UV-curable resist mr-L6000. b,c) CM-AFM height images (z range: 800 nm; image size: 40 μm × 40 μm) of the high-resolution polymer template before (b) and after (c) UV crosslinking, including the average-height cross-sectional analyses. The polymer template was fabricated by CFL on a ca. 150 nm mr-L 6000 layer at 70 °C for 2 h. Subsequently, the template was exposed to a dose of 360 mJ cm^{-2} (at an intensity of 9 mW cm^{-2}), in order to induce crosslinking, on a hotplate at 100 °C for 10 min.

ADVANCED FUNCTIONAL MATERIALS

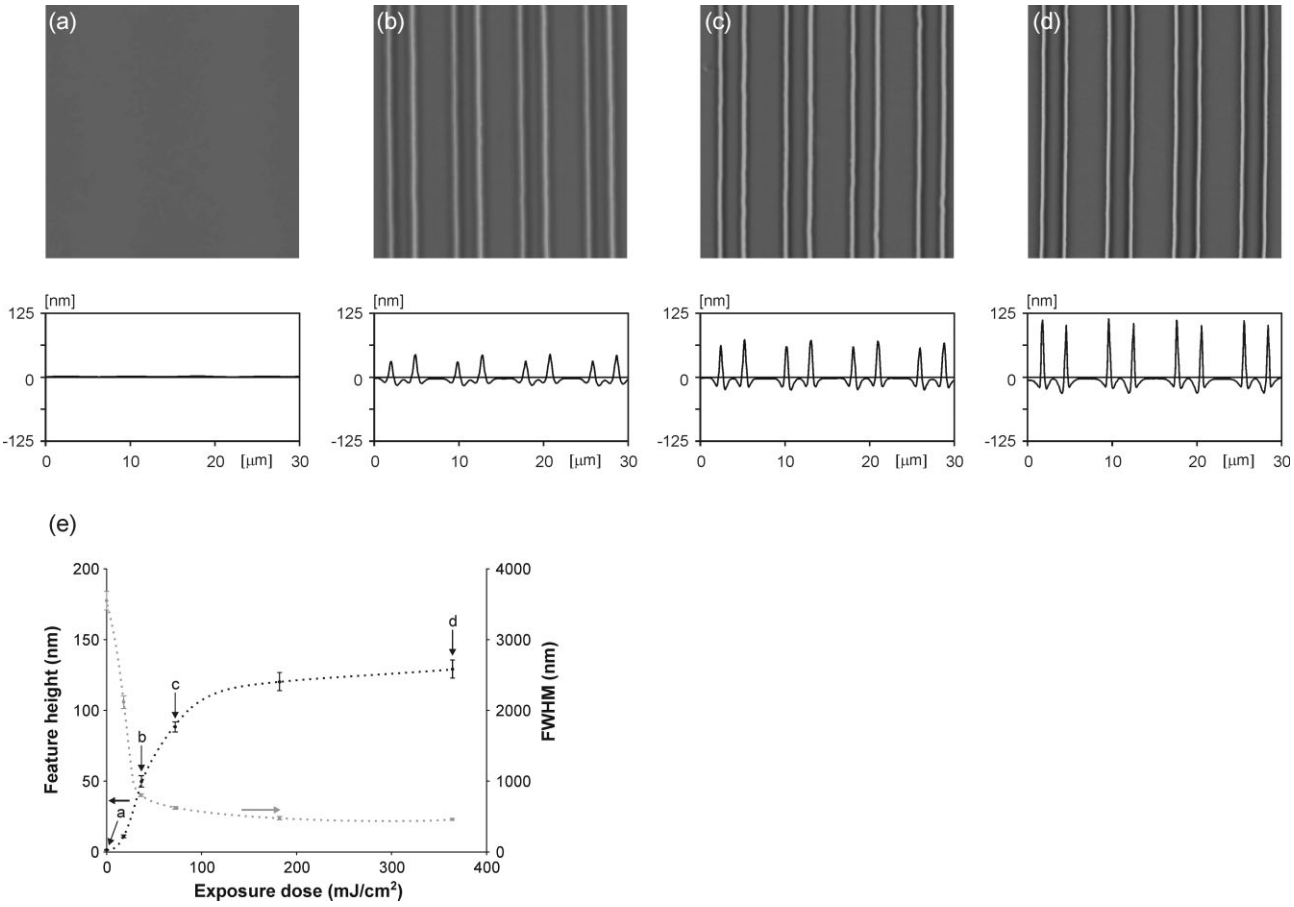

Figure 4. Exposure-dose dependence of the stability of the polymer templates (CFL at 70 °C for 2 h) towards a standard post-exposure bake at 100 °C for 10 min as shown from CM-AFM height images (*z* range: 250 nm; image size: 30 μm × 30 μm), including the average-height cross-sectional analyses, at exposure doses of a) 0, b) 36, c) 72, and d) 360 mJ cm^{-2}; and e) plot of the feature height and FWHM of the polymer template as a function of UV cross-linking. The trend lines in the plot are only drawn as a guide to the eye; a–d refer to the corresponding AFM images above.

mated from the plot (Fig. 4e). Quantitatively, this exposure dose (100 mJ cm^{-2} for 150 nm thick layers) is ca. 33 % larger in comparison to the one determined by dissolution experiments on full resist layers after exposure (500 mJ cm^{-2} for 1 μm thick layers).[20] However, no difference in pattern stability between templates that have undergone a standard post-exposure bake (100 °C for 10 min) and a gradual post-exposure bake[20] (from 30 to 100 °C with a ramp of ca. 4 °C min^{-1}) was found by AFM analysis. This result implies that the initiation of crosslinking on the hotplate is fast on the timescale of thermal flow, and therefore that the rate of crosslinking (resulting in pattern stability) is totally dependent on the exposure dose.

An additional long exposure and hard bake at 120 °C for 10 min were carried out prior to imprinting in PMMA to increase the thermal and mechanical stability further. The structural integrity of the mold was not affected by this hard bake. At a FWHM of ca. 400 nm, the pattern density of the as-fabricated polymer mold was ca. 10 %. For imprinting of such low-pattern-density molds in high-molecular-weight PMMA (M_w = 350 kDa), the NIL conditions were set to 180 °C and 100 bar (1 bar = 10^5 Pa) at an imprint time of 1 min. Figure 5a and b illustrates the high fidelity of NIL as a technique for the pattern replication of the polymer mold in (thermoplastic) PMMA. The feature dimensions of this polymer imprint (Fig. 5b, 120 nm in height and FWHM of 390 nm) approximate the dimensions of the polymer mold (feature height of 125 nm and a FWHM of 400 nm, fabricated by CFL at 70 °C for 4 h).

AFM analysis of the mold during a durability test of tens of imprints (Fig. 5a and c) also illustrates the high mechanical stability of the mold to imprinting under the present conditions. The anti-adhesive properties of this low-density polymer mold were also outstanding. Specific efforts undertaken in the past to eliminate the adhesion of polymer to the mold included the use of ultrathin anti-adhesive layers formed by plasma deposition,[21] anti-adhesion additives in polymers,[22] and the formulation of novel resists and low-surface-energy mold materials. An additive, the formulation of mr-L6000, or a combination of both factors could account for the excellent anti-adhesive properties of the polymer molds during NIL in our case.[23]

In most NIL applications, additive (deposition) or subtractive (etching) post-imprint processing steps usually follow the imprinting step. To use the functionality of the imprint as a template, it is essential to remove the residual polymer layer in the trenches of the imprint by O_2 reactive-ion etching (O_2

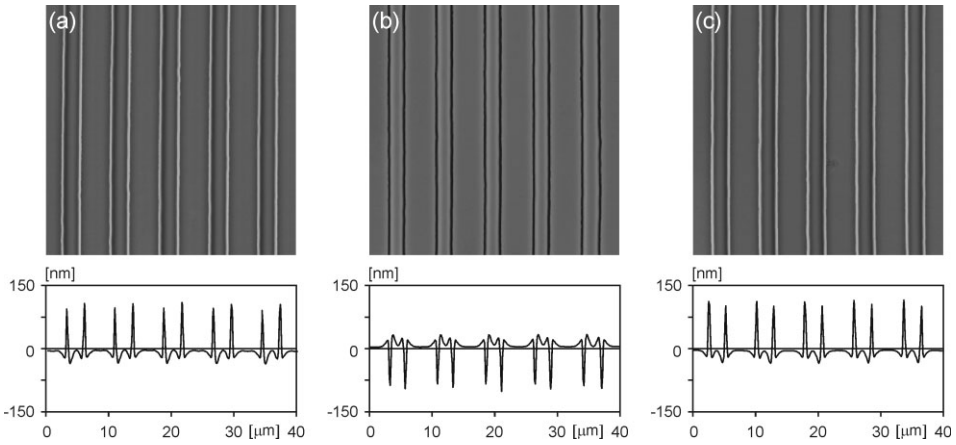

Figure 5. CM-AFM height images (*z* range: 300 nm; image size: 40 μm × 40 μm) of a) the polymer mold, b) an imprint in PMMA, and c) the same polymer mold after tens of imprints at 180 °C and 100 bar, including the average-height cross-sectional analyses.

RIE). The thickness of this residual layer was kept to a minimum by choosing a thickness of the initial PMMA layers (ca. 140 nm) close to the imprint depth of the polymer mold. Cross-sectional AFM analysis of the imprint (Fig. 6a) illustrates a positive taper that is, in general, not the ideal lift-off profile[24] for performing metal lift-off.

To prevent tearing and detachment of the metal during lift-off, metal lift-off on these imprints was performed for thin layers of metal only (ca. 10 % of the imprint depth). Special care was taken to position the substrate perpendicular to the evaporation source during the evaporation of 10 nm of gold. Subsequent sonication in acetone was carried out to remove the polymer template. Gold lines ca. 150 nm wide were fabricated on silicon using this procedure (Fig. 6b). The imprint can also function as an etch mask when imprinting is done on continuous gold layers on silicon substrates. Trenches ca. 150 nm wide were fabricated in gold on silicon by wet-etching of the gold in a basic ferro/ferricyanide-containing etch solution[25] after the O_2 RIE (Fig. 6c). As a result of the positive taper in the PMMA imprint, a discrepancy exists between the feature dimensions of this imprint (after O_2 RIE, FWHM of ca. 400 nm) and the feature dimensions of the metal structures. By changing the time of O_2 RIE treatment, it should, in principle, be feasible to create different opening sizes to the substrate, resulting in a further reduction in the feature dimensions of the metal structures after post-processing (e.g., metal lift-off, or wet-etching) to the sub-100 nm scale. Therefore, these results do not represent the lower limit of this approach, as NIL has been proven to be the most promising technology for the replication of sub-10 nm features.[26]

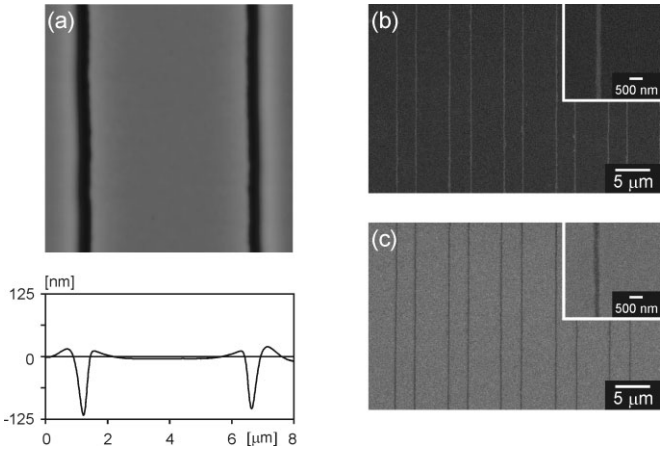

Figure 6. CM-AFM height image (*z* range: 250 nm; image size: 8 μm × 8 μm) of a) a PMMA imprint, including the average-height cross-sectional analysis. The imprint was fabricated by NIL with a UV-cured mr-L6000 mold in 140 nm PMMA at 180 °C and 100 bar. Subsequently, the imprint was exposed to O_2 RIE (50 mTorr (1 Torr = 133.32 Pa), 50 W, 20 sccm O_2, 15–20 s). The processing time was set to over-etch ca. 20 % of the actual residual layer thickness in order to correct for any differences in residual layer thickness over the entire area of the imprint (etch rate of 350 kDa PMMA was ca. 1.7 nm s^{-1}). SEM images of b) 150 nm wide gold lines on silicon after subsequent evaporation of 10 nm of gold and sonication of the substrate in acetone at 40 °C for 15 min and c) 150 nm wide trenches in gold on silicon after wet etching for 10 min and removal of the PMMA in acetone. In the latter case, NIL in PMMA was carried out on 20 nm gold on silicon. Prior to etching, the gold was reduced in absolute ethanol for 30 min. The insets show higher magnification SEM images of an individual feature, for example, a gold line (b) and a trench in the gold layer (c).

2.3. CFL Templates as Etch Masks in Wet-Chemical Etching of Metals

One of the major drawbacks of most polymers is the poor etch resistivity toward O_2 (containing) plasmas. Recently, the highly etch resistant poly(ferrocenylsilanes) (PFS)[27] have been exploited in CFL processing for the direct transfer of the template pattern into silicon by RIE.[28] The requirements for polymer templates to function as etch masks in the wet-chemical etching of metals are, however, not so stringent. This procedure (Fig. 1, route C) differs from the fabrication of μCP masters (Fig. 1, route A) in that CFL of thermoplastic polymers is carried out on 20 nm gold-on-silicon substrates instead of on bare silicon (Fig. 7a). PMMA (M_w = 38 kDa) and PS (M_w = 240 kDa) were used in this procedure.

ADVANCED FUNCTIONAL MATERIALS

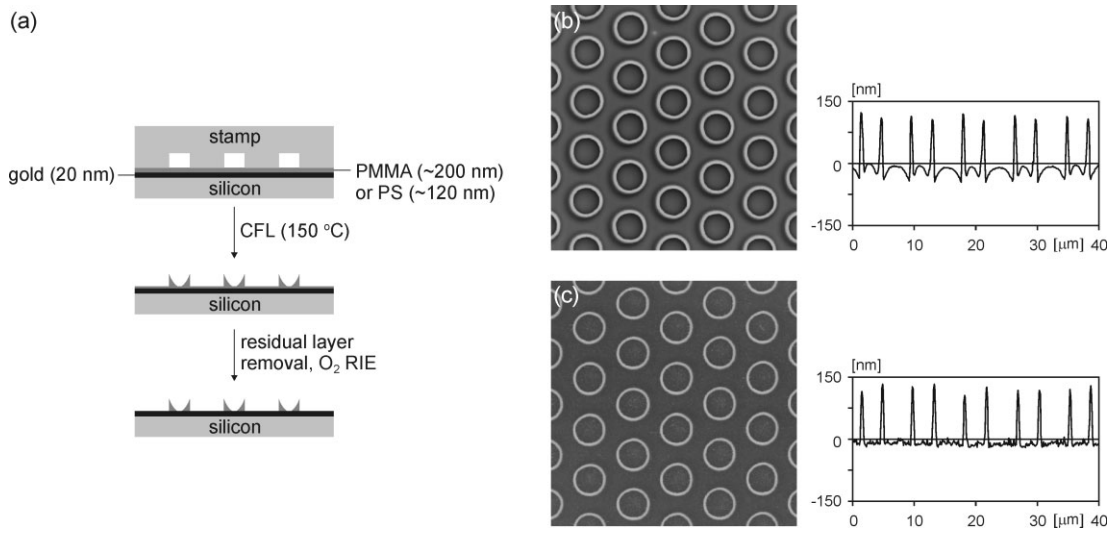

Figure 7. a) Schematic representation of the CFL procedure for the fabrication of polymer (PMMA or PS) etch masks on gold layers on silicon. b,c) CM-AFM height images (*z* range: 300 nm; image size: 40 μm × 40 μm) of a PS template (b) and the corresponding etch mask after residual layer removal (c), including the cross-sectional analyses. The PS template was fabricated by CFL on a ca. 120 nm PS layer at 150 °C for 8 h. Removal of the residual layer was done by O_2 RIE for 2 min in order to expose the underlying gold. The processing time was set to over-etch ca. 20 % of the actual residual layer thickness in order to correct for any differences in residual layer thickness over the entire area of the template.

Cross-sectional AFM analysis of a representative PS template (Fig. 7b) illustrates again the typical transient meniscus (W-shaped) of capillary rise. The present processing conditions result in polymer template features of ca. 180 nm height (FWHM is ca. 480 nm). Attempts to etch the underlying gold were futile, owing to the presence of a residual layer that was protecting the gold. For this template (Fig. 7b), the residual layers were of the order of 80 nm thickness, as determined by an AFM height measurement of the polymer template at a scratch made by a scalpel. Removal of the residual layer without deterioration of the template structures is crucial in the present procedure. The gradual dissolution of the residual polymer in acetone was found to be a convenient and fast procedure, as polymer templates dissolve within about 10–15 s. However, O_2 RIE was chosen instead, in order to have more control over the removal rate of the polymer, which is of the order of nanometers per second. The O_2 RIE etch rates of PS and PMMA were 0.9 and 1.9 nm s^{-1}, respectively, as determined from film-thickness measurements by ellipsometry on full polymer layers upon etching.

A distinct difference in the adhesion of PDMS stamps to PS and PMMA was seen upon cooling the substrate plus stamp, which appeared to result in the clear O_2 RIE rate difference found upon removal of the residual layer. PDMS stamps were found to detach from PS templates within seconds, whereas manual removal of the stamps was necessary in the case of PMMA templates. For the PS templates, removal of the residual layer was feasible at a process time corresponding to the etch rate of this polymer as determined for full layers. From the cross-sectional AFM analysis (Fig. 7c), it is clear that the PS template structure was still intact (in terms of the profile) after O_2 RIE. Additionally, the absolute reduction of ca. 50 nm in feature height and FWHM to ca. 130 nm and ca. 430 nm, respectively, indicates that the O_2 RIE was isotropic. For the PMMA templates, completely removing the residual layer in the former contact areas of the stamp with the PMMA substrate (Fig. 8a and b) was impossible, even after longer etching times.

The contrasting etching behavior of these different polymer templates in O_2 RIE was the starting point for investigating the templates and the polymer-etch rates in more detail by AFM friction analysis, X-ray photoelectron spectroscopy (XPS), and ellipsometry. Only in the case of the PMMA was a significant increase in friction in the contact areas found by AFM friction analysis (Fig. 8c). This is attributed to the transfer of low-molecular-weight silicone residues from the PDMS stamp onto the template during CFL of PMMA. Silicon-containing polymers are known to form thin, nonvolatile silicon oxide (SiO_2) layers at the surface during O_2 plasma exposure, and therefore exhibit a high etch resistance toward O_2 RIE.[29] To examine the transfer of silicone residues and its effect on the polymer etch rate, ca. 150 nm thick PS and PMMA layers were put in contact with two featureless PDMS stamps of different modulus at 150 °C for 8 h (standard CFL conditions). XPS analysis was performed on these layers to determine the amount of silicone transfer, whereas ellipsometry was performed to determine the corresponding etch rate during 20 s of O_2 RIE. The results are summarized in Table 1.

For the PS (C/O 1:0.005) and PMMA (C/O 5:2.01) reference layers, the elemental atomic compositions are in close-to-theoretical quantities (PS C/O = 1:0, PMMA C/O = 5:2). On these reference polymer layers, no Si-containing residues were detected by XPS that could have originated from the environment (e.g., wafer dust, oil vapor from the vacuum pumps). The presence and the position of the Si 2p peak (102.1 eV) on each polymer layer that was in contact with a PDMS stamp indicates

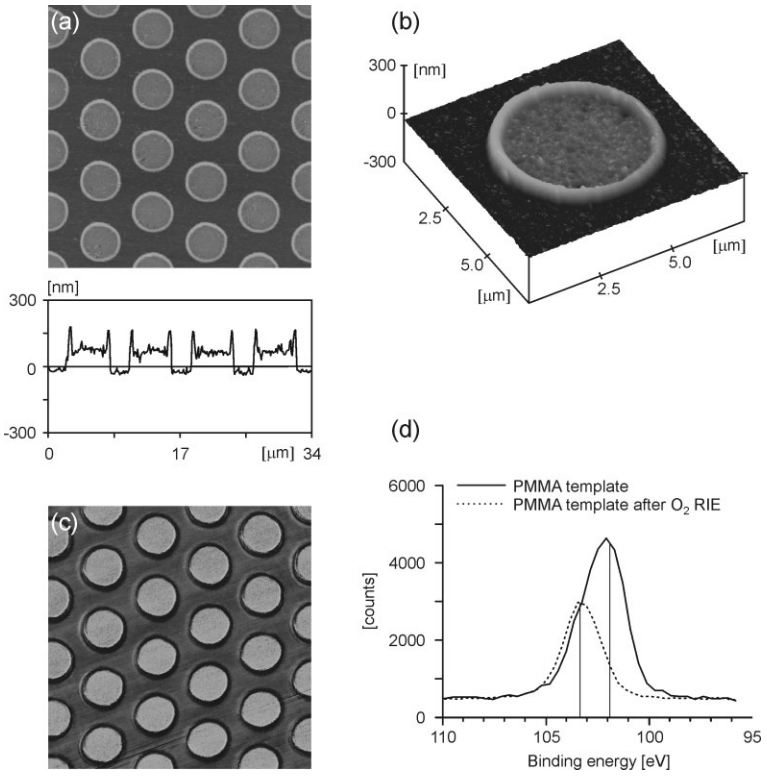

Figure 8. a) CM-AFM height image (*z* range: 600 nm; image size: 34 μm × 34 μm) of a PMMA template (CFL at 150 °C for 8 h) after 100 s of O_2 RIE, including the cross-sectional analysis. b) Three-dimensional CM-AFM height image (*z* range: 600 nm; image size: 7.5 μm × 7.5 μm) of a close-up of one individual PMMA ring. c) CM-AFM friction image of a PMMA template that was in contact with a minimal-modulus PDMS stamp for 8 h at 150 °C prior to O_2 RIE (image size: 34 μm × 34 μm; friction forces [arbitrary units] increase from dark to bright contrast). d) Si 2p XPS spectra of full PMMA layers before and after O_2 RIE. In this typical experiment, the full PMMA layers were in contact with featureless PDMS stamps under the same CFL conditions. The vertical lines in the spectra represent the positions of the Si 2p peak for PDMS (101.8 eV) [30] and SiO_2 (103.3 eV) [34].

Table 1. XPS analysis of polymer substrates versus substrates that were in contact with featureless PDMS stamps under CFL process conditions (150 °C, 8 h), and the corresponding O_2 RIE (50 mTorr, 50 W, 20 sccm O_2, 20 s) rates of these substrates.

		XPS [%]			Etch rate
		C(1s)	O(1s)	Si(2p)	[nm/s]
PMMA	no stamp	71.4	28.6	0.0	1.9
	medium-modulus stamp	67.1	29.1	3.8	1.6
	minimal-modulus stamp	62.4	29.7	8.0	1.4
PS	no stamp	99.5	0.5	0.0	0.87
	medium-modulus stamp	96.8	1.8	1.4	0.81
	minimal-modulus stamp	97.4	1.4	1.3	0.80

that contamination of the polymer surface with Si-containing species from the PDMS stamp (101.8 eV)[30] originates only from the CFL process, irrespective of the type of polymer and the PDMS stamp.

The most important findings of this XPS study are: i) the transfer of Si-containing residues onto PMMA is three to six times higher than in the case of PS; ii) the curing conditions of the PDMS stamp only affect the transfer in the case of PMMA (more curing results in less contamination); and iii) the presence of Si-containing residues on polymer layers compromises the processability of the polymer etch mask to a certain extent during the O_2 RIE, resulting in etch-rate reductions of 8 % for PS and 16–26 % for PMMA. On the basis of the AFM height data in Figure 8a, however, the reduction in etch rate on the PMMA template should have been at least 60 %.[31] This discrepancy suggests, in accordance with a previous study on other systems,[32] that even more Si-containing residues are transferred in the case of stamps containing patterns. The fact that complete inhibition of etching is not seen in the case of PMMA indicates that the amount of Si-containing residues on the surface is not sufficient to form a continuous, etch-protective layer of SiO_2.[33] The clear shift in the Si 2p peak of the Si-containing residues to a higher binding energy (103.4 eV), which is consistent with that of SiO_2[34] (Fig. 8d), and the high surface roughness[35] (ca. 20–40 nm) in the former contact areas (Fig. 7b) upon O_2 plasma exposure support this statement.

On the basis of the processability by O_2 RIE, PS was chosen as the polymer of choice in this procedure. Figure 9b shows an SEM image of 390 nm wide gold rings on silicon after wet-etching of the underlying gold for 10 min. Over-etching and undercutting by isotropic wet-etching are well-known techniques in the semiconductor industry for decreasing feature sizes.[36] Figure 9a shows our over-etching procedure for downscaling the lateral dimensions of the resulting metal structures under the polymer etch mask to the sub-100 nm range (Fig. 9c; average line width: 115 nm).[37]

The basic concept of this procedure is to over-etch the gold from both sides of the sub-micrometer polymer etch mask to obtain high-resolution metal patterns. This procedure is therefore conceptually different from the procedure that exploits the undercut by isotropic wet-etching to transfer the edges of polymer patterns by metal deposition and lift-off.[9] The two SEM images in Figure 9 illustrate the potential of our over-etching procedure, showing the reduction of the lateral dimensions by a factor of 3.6. Additionally, the plot of line width of the gold features versus etch time (Fig. 10a) and further SEM images (Fig. 10b–e) illustrate that high control over the line width of the metal patterns is achieved by controlling the etch time.

The intrinsic etch rate of gold for the basic ferro/ferricyanide-containing etch solution[25] was ca. 3.5 nm min^{-1}, as determined by AFM height analysis of a series of substrates after etching at various times. At the onset of etching, a reduction rate (r) of the line width of about twice the intrinsic etch rate

ADVANCED FUNCTIONAL MATERIALS

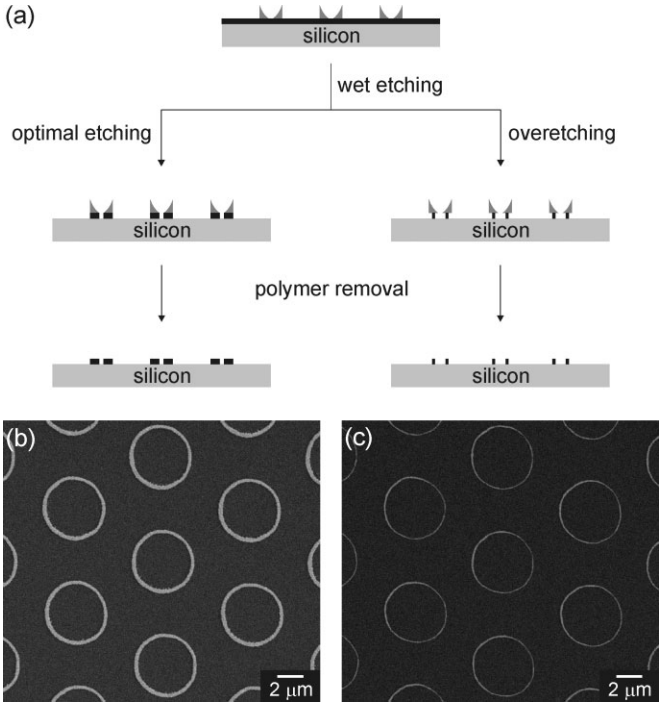

Figure 9. a) Schematic representation of the wet chemical (over-)etching procedure. Prior to wet-etching, the gold was reduced in absolute ethanol for 30 min. b,c) SEM images of gold rings on silicon after 10 and 60 min, respectively, wet-etching of gold at room temperature and subsequent PS removal by sonication in acetone for 10 min.

of gold was estimated from the slope of the plot (Fig. 10a, $r = 7.5$ nm min^{-1}). This rate is consistent with the over-etching of the gold taking place at both sides of the etch mask. However, r decelerated gradually to about 3.6 nm min^{-1} (Fig. 10a). As this etching solution is active for at least several hours, a possible explanation for the etching behavior in this typical procedure is that the inward movement of the etching direction underneath the etch mask limits the diffusion of etchants to the etching front. From a detailed study of this etching solution,[25] it is known that the etch rate is sensitive to changes in the concentration of the coordinating ligand (i.e., thiosulfate) and KOH as, for these electrochemical processes, the oxidation of the gold is the rate-determining step. A reduction in the etch rate by a factor of two, as shown in Figure 10a, was found to correlate to a decrease in concentration of the coordinating ligand by a factor of ten, or to a decrease in concentration of KOH by a factor of five. Since KOH is in large excess, the decrease in the concentration of the coordinating ligand at the etching front is the most-probable cause.

By interpolating the etch curve to the optimal etching time for the 20 nm thick gold layers (ca. 7 min), a line width of ca. 425 nm was found, which is close to the lateral dimensions of the PS etch mask after O_2 plasma treatment (430 nm). Ultimately, gold patterns with line widths of ca. 80 nm have been fabricated with this procedure, although the number of defects in the gold structures increases significantly as the feature sizes approach the grain size of the gold layer.[38]

3. Conclusions

Our results demonstrate that CFL is a convenient and inexpensive technique for fabricating functional, high-resolution polymer templates with high fidelity and excellent uniformity, without the need of advanced lithographic techniques. The successful application of these templates i) as masters for stamp fabrication in soft lithography,[13] ii) as molds for NIL, and iii) as etch masks in the wet-etching of metals illustrates the potential of these templates as tools for high-resolution lithography at the 100 nm scale. Regarding the ultimate resolution, limitations in the critical dimensions of the resultant patterns are set by the heterogeneity in mass transport inherent to these existing pattern-transfer techniques, respectively, alkanethiol inks to metal surfaces, evaporation of metals onto surfaces, and isotropic etching (of polymer templates and metals).

The incorporation of UV-curable mr-L6000 polymer in the CFL procedure has allowed the fabrication of high-stability NIL molds, by UV crosslinking. A constructive modification of this procedure would constitute the crosslinking of the template in situ at the annealing temperature by UV illumination through the (transparent) PDMS stamp after a certain anneal-

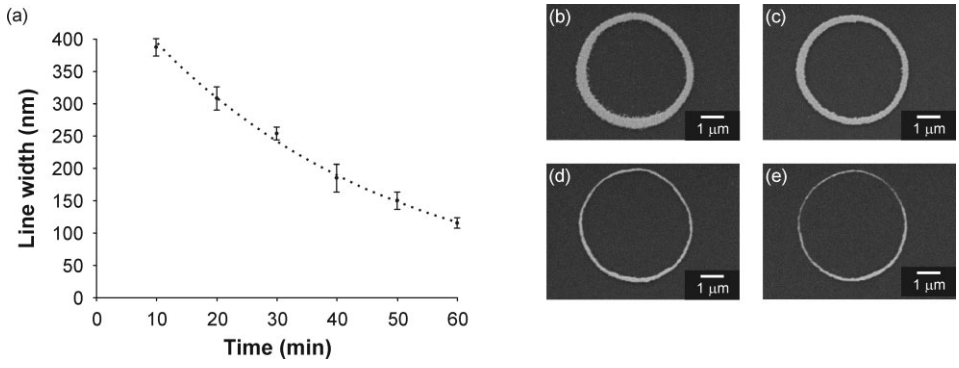

Figure 10. a) Plot of the line width of the gold features versus the etch time at room temperature. The trend line in the plot is only drawn as a guide to the eye. Each data point was calculated from six rings (ten data points per ring) at different locations on the substrate (with a distance of 2.5 mm between each of these rings). b–e) SEM images showing gold rings after wet-etching of the gold for 10, 20, 50, and 60 min, respectively.

ing time. Efforts for developing such a direct UV-CFL procedure or combining CFL and photolithography of UV-curable polymers in the fabrication of multilevel structures have not been further undertaken in this study.

The transfer of PDMS onto the template during CFL was shown by XPS analysis to depend on the curing conditions of the PDMS stamps as well as on the type of polymer. For PMMA and low-modulus PDMS stamps, the transfer of stamp residues was found to severely compromise the O_2 RIE processability of the template in applications that require direct transfer of the template pattern into the underlying substrate (herein, as polymer etch masks for wet-etching of metals). For PS, this was not the case, allowing the residual layer removal and subsequent wet-etching to fabricate 100 nm gold structures.

The key disadvantage of the current set of edge-transfer techniques is that it only allows the fabrication of low-density, straightforward patterns with a feature spacing that is set by the spacing of the original micrometer-size patterns. Although this study has dealt only with regular and periodic structures, CFL is capable of fabricating irregular and more-complex templates without substantial modification of the general procedure, through physical self-organization[39] and dewetting,[16,40] and through capillary dynamics.[41] Application of such processes in CFL could provide new opportunities in the fabrication *and* replication of nanostructures through the combination of top-down and bottom-up approaches.

4. Experimental

Chemicals and Materials: All experiments were carried out in a regular chemical laboratory. Octadecanethiol (ODT), pentaerythritol-tetrakis(3-mercaptopropionate) (PTMP), ethanol, toluene, NaOH, $Na_2S_2O_3$, $K_3Fe(CN)_6$, and $K_4Fe(CN)_6$ were purchased from commercial sources in the highest available purity and used without further purification. A kit of PDMS prepolymer (Sylgard 184 silicone elastomer) and PDMS curing agent (Sylgard silicone elastomer curing agent) was purchased from Dow Corning corporation. PMMA (M_w = 38 kDa and 350 kDa) and PS (M_w = 240 kDa) were purchased from Acros Organics; mr-L6000 was donated by Microresist Technology GmbH, Germany. 100 mm p-type OSP silicon wafers were obtained from Okmetic. Gold layers (20 nm) on titanium-primed (2–3 nm) silicon wafers were purchased from Ssens BV (Hengelo, The Netherlands).

Stamp Preparation: Stamps were fabricated by casting a 10:1 (v/v) mixture of PDMS and curing agent (Sylgard 184, Dow Corning) against a relief pattern of interest (i.e., silicon master or polymer template), cured for 1–18 h at 60 °C, and released at this curing temperature to avoid the buildup of tension due to thermal shrinkage [42]. For CFL, the thickness of these PDMS stamps was about 1 mm to ensure sufficient flexibility.

Polymer-Template Preparation: Silicon substrates of 2 cm × 2 cm were cleaned by ultrasonic treatment in acetone for 15 min and dried in a continuous stream of nitrogen. Polymer solutions were applied onto clean silicon substrates by filtering through a syringe filter with a 0.2 μm poly(tetrafluoroethylene) (PTFE) membrane (Acrodisc CR 25 mm). Spin-coating was performed at 3000 rpm for 30 s in order to obtain polymer layers of 35–200 nm in thickness, followed by a prebake at 100–120 °C for 10 min to remove residual solvent. The stamp and the substrate were equilibrated at the annealing temperature for 30 min, and contact was applied with minimal delay to prevent any dust interference. The stamp plus substrate were left in the oven at about 40 °C above the T_g of the respective polymer for 2–20 h. After cooling for 5 s at room temperature, the PDMS stamp was released from the polymer substrate.

Nanoimprint Lithography: Prior to imprinting, crosslinking of the mr-L6000 polymer template was induced by flood-exposure of the template under a mask aligner (Karl Süss mask aligner MA55) at a dose of 360 mJ cm^{-2} (at an intensity of 9 mW cm^{-2}) and post-exposure baking at 100 °C for 10 min. To function as an NIL mold, additional thermal and mechanical stability was achieved by flood-exposure of this template at 10 kJ cm^{-2} and hard baking at 120 °C for 10 min.

For imprinting the mold pattern into a thermoplastic polymer (PMMA, M_w = 350 kDa), the mold plus polymer substrate was placed in between the plates of a commercial hydraulic press (Specac, 15 tonne manual press equipped with electrical heating plates and a temperature controller) and heated to the imprint temperature of 180 °C (heating rate ca. 35 °C min^{-1}). Upon reaching this imprint temperature, an imprint pressure of 100 bar was applied to pattern the PMMA layer. After 1 min imprinting at 180 °C and 100 bar, the stack was cooled (cooling rate ca. 20 °C min^{-1}) to 106 °C prior to pressure reduction and manual cleavage of the mold from the polymer substrate with a scalpel. The total process cycle (i.e., heating, 1 min imprinting, and cooling) took about 7 min.

Metal evaporation was performed on a commercial evaporation system (Balzers BAK600, E-gun evaporating system). Prior to evaporation, the imprints were exposed to O_2 RIE (50 mTorr (1 Torr = 133.322 Pa), 50 W, 20 sccm O_2) for 15–20 s. The metals were evaporated on the imprint in the following order: chromium (2–3 nm, ca. 1 Å s^{-1} at 2×10^{-6} mbar); gold (10 nm, ca. 1 Å s^{-1} at 3×10^{-6} mbar). Finally, the substrates were sonicated in acetone at 40 °C for 15 min.

Undercutting by Isotropic Wet-Etching: The PS templates were exposed to O_2 RIE (50 mTorr, 50 W, 20 sccm O_2) for 120 s in order to remove the residual layer. The resulting oxide layer on the gold was reduced by leaving the substrates in absolute ethanol for 30 min [43]. Subsequently, etching of the underlying gold was achieved by immersing the templates in an aqueous solution of 1.0 M NaOH, 0.1 M $Na_2S_2O_3$, 0.01 M $K_3Fe(CN)_6$, and 0.001 M $K_4Fe(CN)_6$ for various times at room temperature. (CAUTION: potassium ferricyanide is light sensitive. Photodecomposition releases products that can contain free cyanide. Potassium ferricyanide is also incompatible with acids and liberates HCN.)

Characterization: Polymer film thicknesses were determined with a Plasmos SD 2002 ellipsometer operating at a wavelength of 632.8 nm.

AFM imaging was carried out with a NanoScope III Multimode AFM (Digital Instruments, Santa Barbara, CA) operating in contact mode using Si_3N_4 cantilevers (Nanoprobes, Digital Instruments) with an approximate spring constant of 0.32 N m^{-1}. For height measurements, the scanner was calibrated in the z-direction using a calibration standard with known step height.

Low-resolution SEM imaging was carried out with a JEOL JSM-5610 SEM operating in secondary electron detection. High-resolution SEM imaging was carried out with a LEO Gemini 1550 FEG-SEM.

XPS analyses were carried out with a Physical Electronics Quantum2000 equipped with an Al Kα monochromatic excitation source (source energy = 1486.7 eV, take-off angle set to 45°), a spherical sector analyzer, and a multichannel plate detector (16 detector elements). For the survey scan (pass energy of 224 eV), the X-ray beam was set to 25 W per 100 μm to scan a total area of 700 μm × 300 μm; for element scans (pass energy of 224 eV), the X-ray beam was set to 25 W per 100 μm to scan a total scan area of 700 μm × 300 μm (298 K and $1–3 \times 10^{-8}$ Torr). The sensitivity factors used for C, O, and Si for calculating the atomic concentration were 0.314, 0.733, and 0.368, respectively. The hydrocarbon C 1s signal at 284.8 eV was used as a reference to correct for surface charging.

Received: September 16, 2005
Final version: December 21, 2005
Published online: July 3, 2006

[1] S. J. Holmes, P. H. Michel, M. C. Hakey, *IBM J. Res. Dev.* **1997**, *41*, 7.
[2] J. P. Silverman, *J. Vac. Sci. Technol., B* **1997**, *15*, 2117.
[3] M. A. McCord, *J. Vac. Sci. Technol., B* **1997**, *15*, 2125.

[4] U. S. Tandon, *Vacuum* **1992**, *43*, 241.
[5] Y. Xia, G. M. Whitesides, *Angew. Chem. Int. Ed.* **1998**, *37*, 550.
[6] S. Y. Chou, P. R. Krauss, P. J. Renstrom, *Science* **1996**, *272*, 85.
[7] a) J. A. Rogers, K. E. Paul, R. J. Jackman, G. M. Whitesides, *Appl. Phys. Lett.* **1997**, *70*, 2658. b) T. W. Odom, V. R. Thalladi, J. C. Love, G. M. Whitesides, *J. Am. Chem. Soc.* **2002**, *124*, 12 112.
[8] K. E. Paul, T. L. Breen, J. Aizenberg, G. M. Whitesides, *Appl. Phys. Lett.* **1998**, *73*, 2893.
[9] J. C. Love, K. E. Paul, G. M. Whitesides, *Adv. Mater.* **2001**, *13*, 604.
[10] a) J. Aizenberg, A. J. Black, G. M. Whitesides, *Nature* **1998**, *394*, 868. b) A. J. Black, K. E. Paul, J. Aizenberg, G. M. Whitesides, *J. Am. Chem. Soc.* **1999**, *121*, 8356.
[11] M. Geissler, J. M. McLellan, Y. Xia, *Nano Lett.* **2005**, *5*, 31.
[12] K. Y. Suh, Y. S. Kim, H. H. Lee, *Adv. Mater.* **2001**, *13*, 1386.
[13] C. M. Bruinink, M. Péter, M. de Boer, L. Kuipers, J. Huskens, D. N. Reinhoudt, *Adv. Mater.* **2004**, *16*, 1086.
[14] K. Y. Suh, H. H. Lee, *Adv. Funct. Mater.* **2002**, *12*, 405.
[15] For information on the effect of curing conditions on the material properties of PDMS stamps, see http://www.zurich.ibm.com/st/microcontact/stamps/material.html (accessed September 2005).
[16] K. Y. Suh, J. Park, H. H. Lee, *J. Chem. Phys.* **2002**, *116*, 7714.
[17] K. Y. Suh, P. Kim, H. H. Lee, *Appl. Phys. Lett.* **2004**, *85*, 4019.
[18] K. Y. Suh, S. Chu, H. H. Lee, *J. Micromech. Microeng.* **2005**, *14*, 1185.
[19] K. Y. Suh, P. J. Yoo, H. H. Lee, *Macromolecules* **2002**, *35*, 4414.
[20] M. Wissen, H. Schultz, N. Bogdanski, H.-C. Scheer, Y. Hirai, H. Kikuta, G. Ahrens, F. Reuther, K. Pfeiffer, *Microelectron. Eng.* **2004**, *73*, 184.
[21] R. W. Jaszewski, H. Schift, B. Schnyder, A. Schneuwly, P. Gröning, *Appl. Surf. Sci.* **1999**, *143*, 301.
[22] M. Bender, M. Otto, B. Hadam, B. Spangenberg, H. Kurz, *Microelectron. Eng.* **2002**, *61*, 407.
[23] The presence of fluorine-containing additives that are well known for lowering the surface energy of any surface was excluded by XPS analysis of mr-L6000. Although no specific elements were detected by XPS analysis that could confirm the presence of other types of surfactants in this commercial resist, the product specifications confirm the use of such additives in mr-L6000 (i.e., "surface smoothers") in order to increase the surface smoothness of resist layers in spin-coating. Furthermore, the low pattern density can account in part for the excellent properties of the cured mr-L6000 templates as NIL molds.
[24] B. Faircloth, H. Rohrs, R. Tiberio, R. Ruoff, R. R. Krchnavek, *J. Vac. Sci. Technol., B* **2000**, *18*, 1866.
[25] Y. Xia, X.-M. Zhao, E. Kim, G. M. Whitesides, *Chem. Mater.* **1995**, *7*, 2332.
[26] S. Y. Chou, P. R. Krauss, W. Zhang, L. Guo, L. Zhuang, *J. Vac. Sci. Technol., B.* **1997**, *15*, 2897.
[27] I. Manners, *Chem. Commun.* **1999**, 857.
[28] I. Korczagin, S. Golze, M. A. Hempenius, G. J. Vancso, *Chem. Mater.* **2003**, *15*, 3663.
[29] R. D. Miller, G. M. Wallraff, *Adv. Mater. Opt. Electron.* **1994**, *4*, 95.
[30] G. Beamson, D. Briggs, *High Resolution XPS of Organic Polymers: The Scienta ESCA300 Database*, John Wiley & Sons, Chichester, UK **1992**.
[31] AFM height analysis demonstrates that 80 nm of the 150 nm thick residual layer is still present in the contact areas after 100 s O_2 RIE. Calculations suggest that the AFM height profile in Figure 8a is the result of an etch rate reduction of at least 60 % (from 1.9 to 0.7 nm s^{-1}).
[32] K. Glasmäster, J. Gold, A.-S. Andersson, D. S. Sutherland, B. Kasemo, *Langmuir* **2003**, *19*, 5475.
[33] H. Gokan, Y. Saotome, K. Saigo, F. Watanabe, Y. Ohnishi, in *Polymers for High Technology, Electronics, and Photonics* (Eds: S. R. Turner, M. J. Bowden), ACS Symposium Series, American Chemical Society, Washington, DC **1986**, pp. 358–368.
[34] J. F. Moulder, W. F. Stickle, P. E. Sobol, K. Bomben, *Handbook of X-ray Photoelectron Spectroscopy* (Ed: J. Chastain), Perkin–Elmer Corporation, Eden Prairie, MN **1992**.
[35] V. Z.-H. Chan, E. L. Thomas, J. Frommer, D. Sampson, R. Campbell, D. Miller, C. Hawker, V. Lee, R. D. Miller, *Chem. Mater.* **1998**, *10*, 3895.
[36] W. Kern, C. A. Deckert, in *Thin Film Processes II* (Eds: J. L. Vossen, W. Kern), Academic, Boston, MA **1978**.
[37] At these dimensions, the standard deviation (σ) in the line width of the gold rings is ca. 30 nm: about 50 % of the ring in Figure 9c (and Fig. 10e for close-up SEM image) has lateral dimensions in the sub-100 nm range (> 70 nm).
[38] At these dimensions, the grain size of the metal layer is known to affect the ultimate resolution. For our gold layers, a grain size distribution of 30–60 nm was determined by AFM.
[39] K. Y. Suh, H. H. Lee, *Adv. Mater.* **2002**, *14*, 346.
[40] C. Luo, R. Xing, Y. Han, *Surf. Sci.* **2004**, *552*, 139.
[41] K. Y. Suh, H. H. Lee, *J. Micromech. Microeng.* **2005**, *15*, 400.
[42] H. Schmid, B. Michel, *Macromolecules* **2000**, *33*, 3042.
[43] H. Ron, I. Rubinstein, *Langmuir* **1994**, *10*, 4566.